

## 3.3 Strongly Correlated Quantum Systems

# Numerical Studies on Low-Energy Effective Models for Thin Films of Cuprates by High-Precision Variational Wave Functions

Takahiro Misawa and Masatoshi Imada

*Department of Applied Physics, University of Tokyo*

*Hongo 7-3-1, Bunkyo-ku, Tokyo 113-8656*

Recently, in thin films or interfaces of high- $T_c$  superconductors, many exotic phenomena have been found. For example, in recent experiments on interfaces of a cuprate superconductor,  $\text{La}_2\text{CuO}_4/\text{La}_{2-x}\text{Sr}_x\text{CuO}_4$  [1], unexpected pinning of the  $T_c \sim 42\text{K}$  has been found by systematically changing the doping rates of the metallic phase  $\text{La}_{2-x}\text{Sr}_x\text{CuO}_4$  between  $x = 0.2$  and  $0.5$ . This behavior is in marked contrast with the bulk system where the dome structures of  $T_c$  are established. The discovery has renewed interest in intrinsic nature of the purely two-dimensional  $\text{CuO}_2$  plane, because the superconductivity was shown to occur sharply at a single atomic layer located at the interface.

In this project, to clarify microscopic origin of unconventional pinning of critical temperatures of superconductivities observed at the interfaces of  $\text{La}_2\text{CuO}_4/\text{La}_{2-x}\text{Sr}_x\text{CuO}_4$ , we study multi-layer Hubbard model as a realistic model for interfaces of the cuprates, which is defined by

$$\begin{aligned}
 H = & -t \sum_{\langle i,j \rangle, \sigma, \nu} (c_{i\nu\sigma}^\dagger c_{j\nu\sigma} + \text{h.c.}) \\
 & - t_z \sum_{i, \sigma, \langle \nu, \nu' \rangle} (c_{i\nu\sigma}^\dagger c_{i\nu'\sigma} + \text{h.c.}) \\
 & + U \sum_{i, \nu} n_{i\uparrow} n_{i\downarrow} - \sum_{i\nu} \epsilon_\nu n_{i\nu}, \quad (1)
 \end{aligned}$$

where  $c_{i\nu\sigma}^\dagger$  ( $c_{i\nu\sigma}$ ) is the creation (annihilation) operator of an electron at  $i$ th site on the  $\nu$ th layer with spin  $\sigma$  and  $n_{i\nu\sigma} = c_{i\nu\sigma}^\dagger c_{i\nu\sigma}$  is the

corresponding number operator. For simplicity, we consider only the nearest-neighbor pair for the intra-layer transfer  $t$ . For the inter-layer transfer we take  $t_z = -0.05t$  and the onsite Coulomb interaction is set to  $U = 8t$  as realistic values for the cuprates. The layer-dependent onsite hole level is represented by  $\epsilon_\nu$ , which simulates the effects of the inter-layer diffusion and exchange between La and Sr atoms around the interfaces [2].

For the multi-layer Hubbard model, we have performed high-accuracy many-variable variational Monte Carlo (mVMC) [3-4] calculations. The mVMC method is capable of describing quantum and spatial fluctuations allowing for an accurate estimate of the superconducting stability among competing orders present in strongly correlated systems.

As a result, we have found that carrier densities and superconducting correlations are pinned at the interfaces of the multi-layer Hubbard model in essential agreement with the experimental results. We have shown that the pinning emerges as a result of the inter-layer phase separation. Our result supports that the phase separation and associated enhanced uniform charge fluctuations hold the key to the understanding of the superconductivity in the cuprate superconductors.

## References

- [1] J. Wu *et al.*, Nat. Mat. 12, 877 (2013).

- [2] G. Logvenov, A. Gozar, and I. Bozovic, Science 326, 699 (2009).
- [3] D. Tahara and M. Imada, J. Phys. Soc. Jpn. 77, 114701 (2008).
- [4] T. Misawa and M. Imada, Phys. Rev. B 90, 115137 (2014).

# Theoretical study of novel physics by synergy between electron correlation and spin-orbit coupling

Yukitoshi MOTOME

*Department of Applied Physics,*

*The University of Tokyo, Bunkyo, Tokyo 277-8581*

We have theoretically studied the interplay between charge, spin, and orbital degrees of freedom through strong electron correlations and spin-orbit coupling. This year, we focused on the following three topics. We summarize the main achievements for each topic below.

(i) *Spin dynamics and phase transitions in Kitaev quantum spin liquids:* In some transition metal compounds, such as iridates and rhodates, the interplay between strong electron correlations and spin-orbit coupling brings about an anisotropic, bond-dependent exchange interaction in the Mott insulating state. The peculiar interaction is described by the so-called honeycomb Kitaev model, which has been extensively studied as it provides an exact spin liquid ground state. For clarifying fundamental physics related to the Kitaev model, we have studied the spin dynamics associated with the quantum spin liquid nature. Using the quantum Monte Carlo method and the cluster dynamical mean-field theory, we have calculated the magnetic susceptibility, dynamical spin structure factor, NMR relaxation rate  $T_1$  [1], and Raman scattering spectrum [2]. The results provide the

fingerprints of fractionalization of quantum spins into Majorana fermions. We have also studied the phase transitions from the quantum spin liquid to a long-range ordered state by adding the Ising interaction to the toric code in 2D and 3D (the 2D toric code is the anisotropic limit of the Kitaev model, and the 3D one is its extension to the higher dimension). We found that the system exhibits a peculiar bicritical phase diagram in 3D, while a quantum criticality in 2D [3]. We also published two review articles on the related topics [4,5].

(ii) *Noncoplanar spin configurations with chiral stripes in spin-charge coupled systems:* Noncoplanar spin textures, such as skyrmions, have attracted much attention, as they lead to unconventional transport phenomena through the spin Berry phase mechanism. We have investigated the possibility of new noncoplanar spin textures in itinerant magnets. Employing the Kondo lattice model with classical localized spins, we discovered two different types of noncoplanar spin textures. One is a double- $Q$  state with scalar chirality stripes [5]. This finding has been validated by combination of large-scale numerical simulations, variational

approach, and perturbative expansion. In this noncoplanar state, the chiral stripe gives rise to peculiar alternative helical currents along the stripes. The other is a multiple- $Q$  state composed of a superposition of collinear up-up-down-down states [6]. Taking examples on the square and triangular lattices, we have showed that the multiple- $Q$  states lead to topologically nontrivial states, such as the massless Dirac semimetals and Chern insulators.

(iii) *Charge-spin-orbital fluctuations in mixed valence spinels*: Mixed valence spinels provide a good playground for the interplay between charge, spin, and orbital degrees of freedom in strongly correlated electrons on a geometrically frustrated lattice. Among them,  $\text{AlV}_2\text{O}_4$  and  $\text{LiV}_2\text{O}_4$  exhibit contrasting and puzzling behavior: self-organization of seven-site clusters and heavy fermion behavior. We have performed a comparative study of charge-spin-orbital fluctuations in these two compounds, on the basis of the multiband Hubbard models constructed from the *ab initio* band calculations [7]. Performing the eigenmode analysis of the generalized susceptibility within the random phase approximation, we have found that, in

$\text{AlV}_2\text{O}_4$ , the relevant fluctuation appears in the charge sector in  $\sigma$ -bonding type orbitals. In contrast, in  $\text{LiV}_2\text{O}_4$ , optical-type spin fluctuations in the  $a_{1g}$  orbital are enhanced at an incommensurate wave number at low temperature.

## References

- [1] J. Yoshitake, J. Nasu, and Y. Motome: preprint (arXiv:1602.05253).
- [2] J. Nasu, J. Knolle, D. L. Kovrizhin, Y. Motome, and R. Moessner: preprint (arXiv:1602.05277).
- [3] Y. Kamiya, Y. Kato, J. Nasu, and Y. Motome, Phys. Rev. B **92** (2015) 100403(R).
- [4] 那須 譲治, 宇田川 将文, 求 幸年: 日本物理学会誌 **70** (2015) 776.
- [5] 求 幸年: パリティ **31** (2016) 22.
- [5] R. Ozawa, S. Hayami, K. Barros, G.-W. Chern, Y. Motome, and C. D. Batista: preprint (arXiv:1510.06830).
- [6] S. Hayami, R. Ozawa, and Y. Motome, preprint (arXiv:1603.06646).
- [7] A. Uehara, H. Shinaoka, and Y. Motome: Phys. Rev. **92** (2015) 195150.

# Analysis of an effective model with valence skipping effect using dynamical mean field theory

Akihisa Koga

*Department of Physics, Tokyo Institute of Technology  
Ookayama, Meguro, Tokyo 152-8551*

Colossal negative thermal expansion in the nickel oxide  $\text{BiNiO}_3$  is recently found [1]. This phenomenon is considered to originate from the “valence skipping” nature of Bi ions and strong electron correlations intrinsic in Ni ions. Due to the valence skipping effect, at low temperature, the material is the insulator showing the characteristic valence as  $\text{Bi}_{0.5}^{3+}\text{Bi}_{0.5}^{5+}\text{Ni}^{2+}\text{O}_3$ . By applying pressure, it changes to  $\text{Bi}^{3+}\text{Ni}^{3+}\text{O}_3$ , which is accompanied by a discontinuous volume shrinkage. In order to clarify the relation between the thermal expansion and valence skipping nature, an effective model with Coulomb interactions was analyzed by Hartree-Fock approximation [2].

In the present study, we address the Hubbard model, where the valence skipping nature in Bi ions and orbital degeneracy in Ni ions are taken into account. The schematic picture of this model is presented in Fig. 1. By applying dynamical mean-field theory and the continuous quantum Monte Carlo simulation to the model, we systematically examine the effect of the electron correlation in this model. In the Monte Carlo simulation, we use the ALPS library preinstalled in System B of the ISSP supercomputer system [3]. This library provides us with efficient parallelization in the Monte Carlo sampling.

Using the above technique, we newly find ferromagnetic and antiferro-orbital ordered phases due to the existence of the orbital degeneracy [4], in addition to charge ordered and antiferromagnetic phases discussed in the pre-

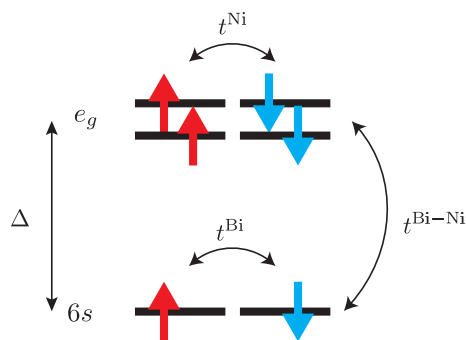


Figure 1: Schematic picture of the Hubbard model that we addressed.

vious study [2]. The states that we find are stabilized in the case with the strong Coulomb interaction. We expect that the ferromagnetic and orbital ordered states could be experimentally observed at low temperatures.

## References

- [1] M. Azuma, W. Chen, H. Seki, M. Czap-ski, S. Olga, K. Oka, M. Mizumaki, T. Watanuki, N. Ishimatsu, N. Kawamura, S. Ishiwata, M. G. Tucker, Y. Shimakawa, and J. P. Attfield: *Nat. Comm.* **2** (2011) 347.
- [2] M. Naka, H. Seo, and Y. Motome: *Phys. Rev. Lett.* **116**, (2016) 056402.
- [3] B. Bauer *et al.*: *J. Stat. Mech.* **2011** (2011) P05001.
- [4] S. Kojima, J. Nasu, and A. Koga: arXiv:1602.07831.

# Photoinduced phase transitions in strongly correlated superconductors

Hideo AOKI

*Department of Physics, University of Tokyo  
Hongo, Tokyo 113-0033*

## FLEX+DMFT approach to the d-wave superconductivity[1]

The two-dimensional repulsive Hubbard model still harbours fundamental questions, among which is how the “ $T_c$  dome” in the phase diagram against the band filling can be understood. We have combined the dynamical mean field theory (DMFT) with the fluctuation exchange approximation (FLEX) to investigate strongly correlated systems, especially to obtain a phase diagram for d-wave superconductors[1]. The DMFT+FLEX method, which can also be viewed as a proposal for a new Luttinger-Ward functional, incorporates the momentum-dependent pairing interaction treated in FLEX into DMFT which can describe Mott’s insulator, so that the method can describe anisotropic pairings along with the local correlation effects (Mott physics). We have applied the formalism to the two-dimensional repulsive Hubbard model to obtain a phase diagram. The result does indeed exhibit a superconducting  $T_c$ -dome against band filling, both in the absence and presence of the Fermi surface warping ( $t'$ ). We have traced back the origin of the dome to the local vertex correction from DMFT that gives a filling-dependence in the FLEX self-energy.

## Light-induced collective Higgs mode in superconductors[2]

A superconductor illuminated by an ac electric field with frequency  $\Omega$  poses an interesting problem. We have theoretically found that the

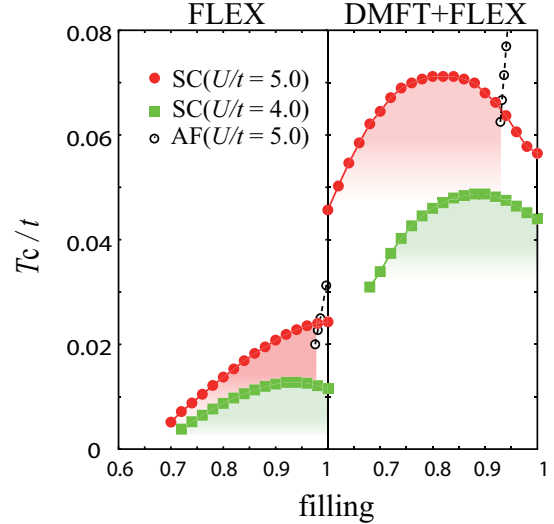


Figure 1:  $T_c$  vs band filling in FLEX (left panel) and in DMFT+FLEX (right) for different values of the Hubbard  $U$ . [1].

ac modulation generates a collective precession of Anderson’s pseudospins, hence a coherent amplitude oscillation of the order parameter, in the BCS state with a doubled frequency  $2\Omega$  through a nonlinear light-matter coupling[2]. We have formulated the problem in a mean-field to show that the induced pseudospin precession resonates with the Higgs amplitude mode of the superconductor at  $2\Omega = 2\Delta$  with  $2\Delta$  being the superconducting gap. The resonant precession is accompanied by an enhancement of the third-harmonic generation. We have further explored the effect of electron-electron scattering on the pseudospin reso-

nance by applying the nonequilibrium dynamical mean-field theory (DMFT) to the attractive Hubbard model driven by ac electric fields. The result indicates that the pseudospin resonance is robust, although the resonance width is broadened due to electron scattering, which determines the lifetime of the Higgs mode.

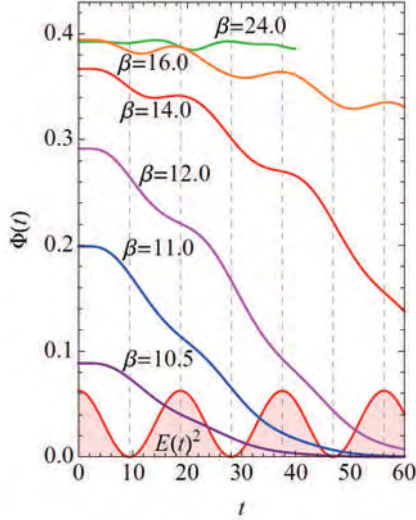


Figure 2: Temporal evolution of the superconducting order parameter  $\Phi(t)$  calculated with the nonequilibrium DMFT for the attractive Hubbard model at half filling driven by the ac field with the infinite-dimensional density of states,  $U = 2.25$ ,  $A = 0.2$ , and  $\Omega = 2\pi/37.5$ , for several temperatures ( $\beta^{-1}$ ) for the initial states. The sinusoidal curve represents  $E(t)^2 \propto \cos^2 \Omega t$ . [2].

### Collective amplitude modes in strongly-coupled superconductors [3]

We have studied collective amplitude modes of the superconducting order parameter in strongly-coupled electron-phonon systems described by the Holstein model using the nonequilibrium DMFT with the self-consistent Migdal approximation as an impurity solver [3]. The frequency of the Higgs amplitude mode is found to coincide with the superconducting gap even in the strongly-coupled (beyond BCS) regime. Besides the Higgs mode, we find another collective mode involving the dynam-

ics of both the phonon and the superconducting order parameter, which reflects a strong *electron-mediated phonon-phonon interaction*. We predict that these should be observed in time-resolved photoemission spectra.

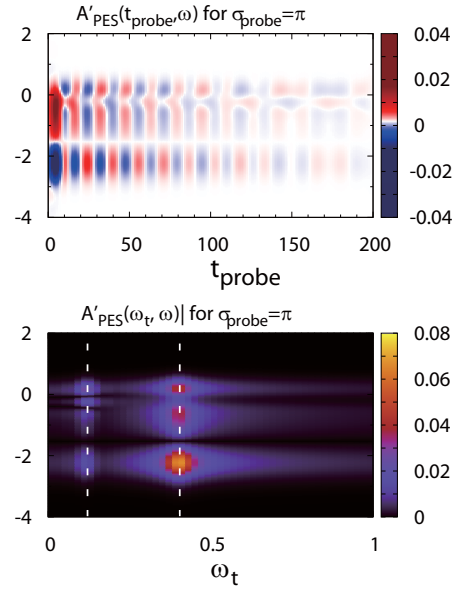


Figure 3: The spectral function  $A(t, \omega)$  against  $t$  and  $\omega$  and its Fourier transform. White vertical lines indicate the frequencies,  $\omega_H$  and  $\omega_{H2}$ , of the two collective modes. [3]

## References

- [1] M. Kitatani, N. Tsuji, H. Aoki: FLEX+DMFT approach to the d-wave superconducting phase diagram of the two-dimensional Hubbard model, *Phys. Rev. B* **92**, 085104 (2015).
- [2] Naoto Tsuji and Hideo Aoki: Theory of Anderson pseudospin resonance with Higgs mode in a superconductor, *Phys. Rev. B* **92**, 064508 (2015).
- [3] Yuta Murakami, Philipp Werner, Naoto Tsuji and Hideo Aoki: Multiple amplitude modes in strongly coupled phonon-mediated superconductors, *Phys. Rev. B* **93**, 094509 (2016).

# Topological insulators in heavy-fermion systems

Tsuneya Yoshida

*Department of Physics, Kyoto University, Kyoto 606-8502, Japan  
Sakyo-ku, Kyoto 606-8502, Japan*

Topological insulators attract much interest[1]. The electronic state of this system has nontrivial topology which predicts gapless excitations at the edge/surface. These gapless excitations are source of interesting phenomena; e.g., topological magnetoelectric effects and emergence of Majorana fermions. So far topological insulators are studied as free fermion systems. Recently, however, it has been pointed out that topological insulators can be realized in heavy-fermion systems where electron correlations are strong. In these systems, electron correlations and topology are expected to induce novel phenomena, and thus, understanding correlation effects on topological insulators is one of the important issues of this field.

In our study, we have analyzed heavy fermion systems having nontrivial topology. In particular, we have addressed temperature effects on topological Kondo insulators. Firstly, we have performed model calculation[2] by using real-space dynamical mean field theory (r-DMFT) combined with numerical renormalization group method. After that we addressed more detailed analysis[3]; LDA+DMFT is applied to SmB<sub>6</sub> which is a promising candidate for the topological Kondo insulator. In order to perform the large-scale numerical calculation, we have fully made use of the supercomputer resource at ISSP.

In Ref. [2], we have analyzed the Kane-Mele-Kondo lattice which is two-dimensional. With this method, we can study wide range of temperature[4], from  $T \sim 10^{-4}t$  to  $T \sim 10^{-1}t$ . Here the bandwidth of the conduction electron

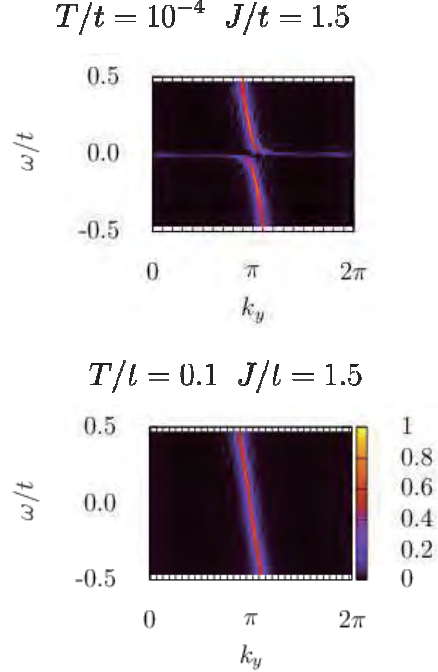


Figure 1: Gapless edge modes appearing at finite temperatures. Top and bottom panels represent data for  $T = 0.1t$

is approximately  $6t$ .

As the result of the detailed analysis, we have found that gapless edge modes are restored by temperature effects. Around zero temperature, the Kondo effect is dominant and destroys topological structure. Correspondingly edge modes are gapped. With increasing temperature, however, the Kondo effect is suppressed and gapless edge modes are restored. We have observed this behavior by direct calculation of edge modes as well as the calculation of topological response in the bulk.

The restoration of gapless edge modes in finite temperature region is observed in Fig. 1. In this figure, we can see that edge modes are destroyed for  $T = 10^{-4}t$ , while the gapless modes are restored  $T = 10^{-4}t$  and  $T = 10^{-1}t$ , respectively.

Furthermore, we have applied LDA+DMFT to  $\text{SmB}_6$  [3]. Concerning the group velocity of this compound, two different experiments have reported different values; according to a transport measurement, the group velocity is  $v \sim 200\text{meV}\text{\AA}$ , while it is  $v \sim 4\text{meV}\text{\AA}$  according to an ARPES measurement. We have addressed this puzzle. Our study has elucidated that interplay between the Kondo effect and temperature drastically changes the group velocity (or, the renormalization factor) in gapless edge modes in the topological Kondo insulator  $\text{SmB}_6$ . We conclude that this interplay explains the puzzle of the above two experiment since transport and ARPES measurement have been carried out at  $T = 3\text{K}$  and  $T = 17\text{K}$ , respectively. This results is consistent with the slave-boson analysis in Ref. [5].

## References

- [1] M. Z. Hasan *et al.*, Rev. Mod. Phys. **82**, (2010) 3045-3067.; X. L. Qi *et al.*, Rev. Mod. Phys. **83**, (2011) 1057.
- [2] T. Yoshida, R. Peters, and N. Kawakami: Phys. Rev. B **93**, (2016) 045138.
- [3] R. Peters, T. Yoshida, H. Sakakibara, and N. Kawakami: arXiv:1510.06476
- [4] R. Peters and N. Kawakami: Phys. Rev. B **92**, (2015) 075103.
- [5] V. Alexandrov, *et al.*: Phys. Rev. Lett. **114**, (2015) 177202.

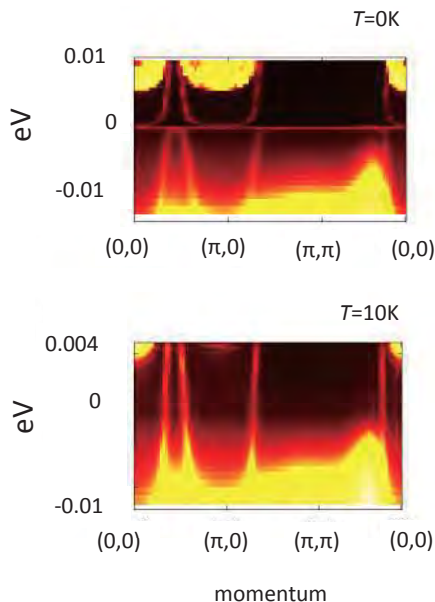


Figure 2: Surface state of  $\text{SmB}_6$ .

# Effect of apical oxygen phonon on $d$ -wave superconductivity

Takahiro OHGOE

*Department of Applied Physics, The University of Tokyo,*

*7-3-1 Hongo, Bunkyo-ku, Tokyo 113-0033*

Despite intensive studies on high- $T_c$  cuprate, its mechanism of the superconductivity is still controversial. ARPES experiments [1] demonstrated indications of strong electron-phonon interactions. Motivated by these results, some theoretical works proposed scenarios that electron-phonon interactions enhance  $d$ -wave superconductivity[2,3]. However, the role of electron-phonon interactions in cuprates remains unclear.

In this work, we studied  $d$ -wave superconductivity in the Holstein-Hubbard model by using the many-variable variational Monte Carlo method[4,5]. We performed simulations in system B by using a flat MPI or OpenMP+MPI parallelization. The Holstein phonon can be viewed as a simplified electron-phonon interaction of apical oxygen in cuprates. Our simulation results showed that physical quantities are insensitive to Holstein phonons [Fig.1(a)]. In the next step, we considered the effect of the off-site part of the electron-phonon interaction  $g'$  which introduces phonon-mediated off-site attractions between electrons. As a result, we found that the off-site electron-phonon interaction increases the condensation energy [Fig.(b)], and thus a  $d$ -wave

superconducting state becomes more stable energetically.

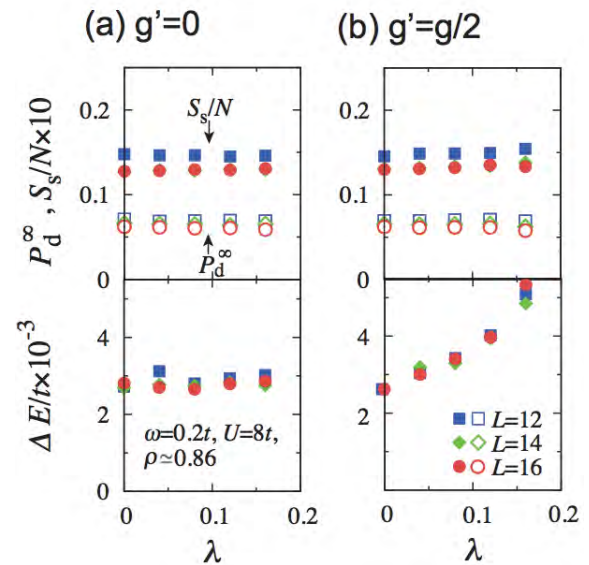


Fig. 1: Physical quantities (long-range part of  $d$ -wave superconducting correlation function  $P_d^\infty$ , spin structure factor  $S_s(\pi, \pi)$ , and the condensation energy  $\Delta E$ ) as functions of the dimensionless electron phonon interaction  $\lambda$ .

## References

- [1] A. Lanzara *et. al*, Nature **412**, 510 (2001)
- [2] S. Ishihara and N. Nagaosa, Phys. Rev. B **69**, 144520 (2004)
- [3] Z. B. Huang *et. al*, PRB **68**, 220507 (2003)
- [4] D. Tahara and M. Imada, J. Phys. Soc. Jpn. **77**, 1140701 (2008)
- [5] T. Ohgoe and M. Imada, Phys. Rev. B **89**, 195139(2014)

# Improvement of many-variable variational Monte Carlo method and its application to iron-based superconductors

Takahiro Misawa

*Institute for Solid State Physics, The University of Tokyo  
Kashiwa, Chiba 277-8581, Japan*

In this project, to improve the accuracy of the many-variable Monte Carlo method (mVMC), we implement the backflow wave function based on the Pfaffian wave function and the multi-Pfaffian method, which superposes the many-body wave functions. We have also analyzed low-energy effective models for iron-based superconductors FeTe and FeSe by using the mVMC.

Before explaining the details of the backflow wave functions, we briefly explain the wavefunctions used in the mVMC method. Our wave function is defined as

$$|\psi\rangle = \mathcal{P}|\phi_{\text{pair}}\rangle, \quad (1)$$

$$|\phi_{\text{pair}}\rangle = \left(f_{ij}c_{i\uparrow}^\dagger c_{j\downarrow}^\dagger\right)^{N_e/2}|0\rangle, \quad (2)$$

where  $f_{ij}$  is variational parameter and  $c_{i\sigma}^\dagger$  ( $c_{i\sigma}$ ) is a creation (annihilation) operator of an electron with spin  $\sigma$  on the  $i$ th site.  $N_e$  represents the number of electrons. By properly optimizing the variational parameter  $f_{ij}$ , we can describe several different states such as antiferromagnetic orders, charge-ordered states, correlated paramagnetic metals, and superconducting phases. To include the many-body correlations, we introduce correlation factors  $\mathcal{P}$  such as Gutzwiller or Jastrow factors. Details of mVMC method are explained in the literature [1, 2].

L. Tocchio and co-workers introduce the backflow wavefunctions in the conventional

Slater-type wave function as follows [3]

$$|\phi_{\text{bf}}\rangle = \prod_{\sigma,n=1}^{N_e/2} \left(\sum_i \tilde{\Phi}_{in\sigma} c_{i\sigma}^\dagger\right)|0\rangle, \quad (3)$$

$$\tilde{\Phi}_{in\sigma} = \Phi_{in\sigma} + \sum_k \eta_k(D, H)\Phi_{k\sigma}, \quad (4)$$

where  $\Phi_{in\sigma}$  is the coefficient of the Slater-type wave function and  $\eta_k(D, H)$  is the variational parameter that depends on the number of doublon ( $D$ ) and holon ( $H$ ). It is shown that backflow correlations improve the accuracy of the wave functions [3].

We extend this Slater-type backflow wavefunctions to Pfaffian-type wave functions as follows [4, 5]

$$|\psi_{\text{pair-bf}}\rangle = \left(\tilde{f}_{ij}c_{i\uparrow}^\dagger c_{j\downarrow}^\dagger\right)^{N_e/2}|0\rangle, \quad (5)$$

$$\tilde{f}_{ij} = \sum_n \tilde{\Phi}_{in\uparrow}\tilde{\Phi}_{jn\downarrow}. \quad (6)$$

We have also shown that wavefunctions are systematically improved by superposing the many-body wavefunctions (multi-Pfaffian method) as follows [5]

$$|\psi\rangle = \sum_{n=1}^{N_{\text{Pf}}} \mathcal{P}_n|\phi_n\rangle, \quad (7)$$

where  $N_{\text{Pf}}$  is the number of independent many-body wavefunctions.

By using the improved wave functions, we have shown that the accurate finite-temperature calculation based on the imaginary time evolution is possible in the mVMC method [5].

In the analysis of the iron-based superconductors [6], we first derive the low-energy effective model by using the ab initio downfolding method. In this method, we evaluate the transfer integrals and interaction parameters based on the ab initio band calculations. To eliminate the double counting of the correlation effects that exists in the conventional ab initio downfolding scheme, we perform the constrained GW calculations. By solving the low-energy effective model, we show that elimination of the double counting plays an essential role in stabilizing the bicollinear magnetic order in FeTe. We also solve the low-energy effective model for FeSe and find the peculiar degeneracy of the several magnetic orders occurs in FeSe. We have pointed out that this peculiar degeneracy may be the origin of the exotic phenomena found in FeSe. Further analysis of the low-energy effective models by using the improved wavefunctions such as backflow wavefunction is intriguing issue but left for future study.

## References

- [1] D. Tahara and M. Imada, *J. Phys. Soc. Jpn.* **77**, 114701 (2008).
- [2] T. Misawa and M. Imada, *Phys. Rev. B* **90**, 115137 (2014).
- [3] L. F. Tocchio, F. Becca, and C. Gros, *Phys. Rev. B* **83**, 195138 (2011).
- [4] K. Ido, T. Ohgoe, and M. Imada, *Phys. Rev. B* **92**, 245106 (2015).
- [5] K. Takai, K. Ido, T. Misawa, Y. Yamaji, and M. Imada, *J. Phys. Soc. Jpn.* **85**, 034601 (2016).
- [6] M. Hirayama, T. Misawa, K. Miyake, and M. Imada, *J. Phys. Soc. Jpn.* **84**, 093703 (2015).

# Numerical study of critical phenomena in strongly correlated Dirac electrons

Yuichi OTSUKA

*RIKEN Advanced Institute for Computational Science  
Kobe, Hyogo 650-0047*

Dirac electrons offer suitable test beds where we can study interaction-driven phase transitions by means of unbiased numerical methods. In our previous studies [1, 2], we have elucidated the quantum critical behavior of the Mott transition occurred in the Hubbard model on the honeycomb lattice and on the square lattice with  $\pi$  flux penetrating each plaquette, both of which constitute the massless Dirac dispersions in the non-interacting limit. These works were initially motivated by the possible Mott metal-insulator transition expected to occur in graphene-like materials. However, it has been recently recognized that the interaction-driven transitions in the Dirac fermions have more general and universal aspects, which can be interpreted in terms of the Gross-Neveu (GN) model, a model extensively studied in quantum field theory [3].

The semimetal (SM) to Mott insulator transition accompanied by the antiferromagnetic (AF) transition, which we have studied in the Hubbard model on the honeycomb lattice and the square lattice with  $\pi$ -flux, corresponds to the breaking of the chiral- $SU(2)$  symmetry in the context of the GN model. On the other hand, the transition from SM to the charge-density-wave phase, which has been recently investigated in the spinless  $t$ - $V$  model on the same lattices [4], is categorized as the chiral- $Z_2$  symmetry breaking. The purpose of this project is to clarify the critical phenomena in the strongly correlated Dirac fermions classified with the chiral- $XY$  symmetry, which is

the one remaining class out of the known three categories in the GN model.

We have performed large-scale quantum Monte Carlo (QMC) simulations for the attractive Hubbard model on the triangular lattice, to which the staggered  $\pi$ -flux is added to constitute the Dirac dispersion in the non-interacting limit as shown in Fig. 1. In this model, since the lattice structure is not bipartite, we expect the only  $U(1)$  symmetry is broken even at half-filling. In addition, the QMC simulation is not vexed by the negative-sign problem in the case of the attractive (negative  $U$ ) model. We have utilized the QMC code that we have highly optimized on the K computer and the FX10 system. The simulations for small to intermediate clusters with linear system size  $L \leq 24$  were done on the system B, and those with  $L = 32, 40$  were performed on the system C.

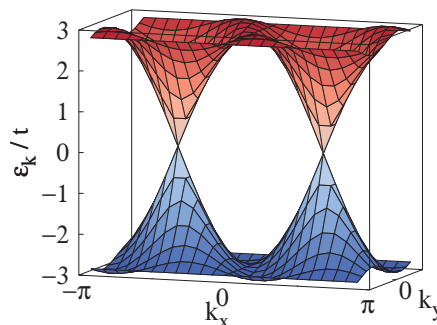


Figure 1: Non-interacting energy dispersion of triangular lattice with staggered  $\pi$ -flux.

We have calculated the pairing correlation

function on each finite-size cluster,  $P_s(L) = \frac{1}{N} \sum_{ij} \langle \Delta_i^\dagger \Delta_j + \Delta_i \Delta_j^\dagger \rangle$ , where  $\Delta_i^\dagger = c_{i\uparrow}^\dagger c_{i\downarrow}^\dagger$ , and extrapolated them to the thermodynamic-limit to obtain the superconducting (SC) order parameters,  $\Delta = \lim_{L \rightarrow \infty} P_s(L)$ . In addition, the quasiparticle weight  $Z$  is estimated from jump of the momentum distribution function at the Fermi level. Both of these observables show that the SM to SC transition occurs at  $U_c/t = 7.0 \pm 0.1$  as shown in Fig. 2. More detailed analysis on evaluation of the critical exponents is ongoing.

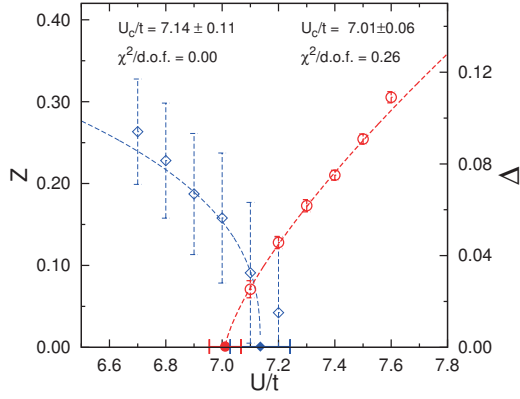


Figure 2:  $|U|/t$ -dependence of quasiparticle weight  $Z$  and superconducting order parameter  $\Delta$ .

## References

- [1] S. Sorella, Y. Otsuka, and S. Yunoki: Sci. Rep. **2** (2012) 992.
- [2] Y. Otsuka, S. Yunoki, and S. Sorella: Phys. Rev. X. **6** (2016) 011029.
- [3] D. Gross and A. Neveu: Phys. Rev. D. **10** (1974) 3235.
- [4] L. Wang, P. Corboz, and M. Troyer: N. J. Phys. **16** (2014) 103008.

# Density-matrix renormalization group method for quantum impurity models

Tomonori SHIRAKAWA

*RIKEN Center for Emergent Matter Science (CEMS)*

*Wako, Saitama 351-0198, Japan*

We have introduced the density matrix renormalization group method (DMRG) as a solver for quantum impurity models, such as Anderson impurity models and Kondo impurity models [1]. The DMRG is advantageous for other impurity solvers when applied to quantum impurity models. First of all, unlike the quantum Monte Carlo methods, the DMRG is able to obtain directly the full spectral function in real frequency without analytical continuation. Secondly, the DMRG can readily calculate the entanglement properties.

Here, to demonstrate the power of the method, we apply it to the single-impurity Anderson model on the honeycomb lattice [2]. Our result shows that the phase diagram contains two distinct phases, the local moment phase (LM) and the asymmetric strong coupling (ASC) phase (See Fig. 1 (a)). We compare the results with those for the low-energy effective pseudogap Anderson model. We find that the ground state phase diagram and the asymptotically low-energy excitations for these two models are found to be in excellent quantitative agreement, thus providing a quantitative justification for the previous studies based on low-energy approximate approaches.

Futhermore, we find that the lowest entanglement level  $\xi_i$  ( $\xi_1 \leq \xi_2 \leq \dots$ ) is doubly degenerate for the LM phase, whereas it is singlet for the ASC phase. Because of this qualitatively different behavior, we can consider the gap of the entanglement spectrum,  $\Delta\xi = \xi_2 - \xi_1$ , as an order parameter to distin-

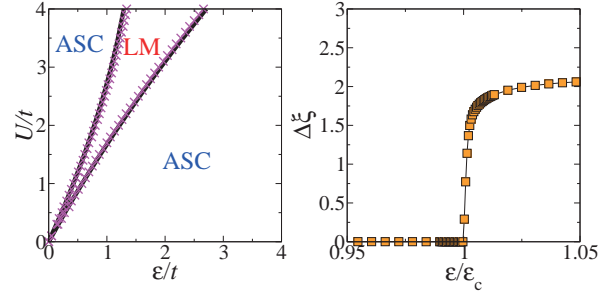


Figure 1: (a) Ground state phase diagram for the single-impurity Anderson model on the honeycomb lattice (symbol) and the pseudogap Anderson model (solid line).  $\varepsilon$  and  $U$  correspond to the on-site potential and Coulomb interaction at impurity site, respectively. (b) Gap of the entanglement spectrum,  $\Delta\xi = \xi_2 - \xi_1$ .  $\varepsilon_c$  is determined from (a).

guish the different phases. Indeed, the phase boundary determined from  $\Delta\xi$  is the same as the one determined from the local quantities at the impurity site. This clearly demonstrates that  $\Delta\xi$  serves as a quantity to determine the phase boundary of the impurity quantum phase transition.

## References

- [1] T. Shirakawa and S. Yunoki: Phys. Rev. B **90** (2014) 195109.
- [2] T. Shirakawa and S. Yunoki: arXiv:1604.00721.

# First-principles study of the iron-based ladder compound $\text{BaFe}_2\text{S}_3$

Ryotaro ARITA

*RIKEN Center for Emergent Matter Science*

*Wako, Saitama, 351-0198*

Recently, it has been reported that the two-leg ladder compound  $\text{BaFe}_2\text{S}_3$  (Fig.1) becomes a superconductor under high pressure[1, 2]. Motivated by this discovery, we performed a first-principle calculation and investigated the electronic and magnetic properties of this compound[3]. We found that the magnetic alignment in which the spins are coupled ferromagnetically along the rung and antiferromagnetically along the leg is the most stable in the possible magnetic structure. This result is consistent with the experiment.

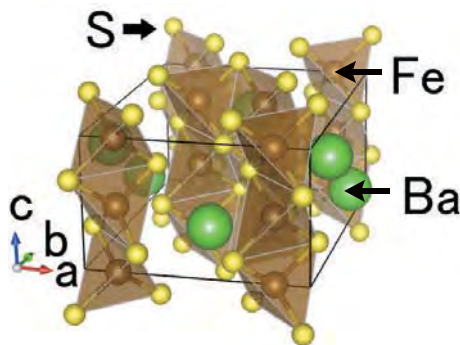


Figure 1: Crystal Structure of  $\text{BaFe}_2\text{S}_3$ .

We then derived an effective low-energy model[4] by means of the *ab initio* downfolding method. We found that the complex band structure around the Fermi level is represented only by the Fe  $3d_{xz}$  (mixed with  $3d_{xy}$ ) and  $3d_{x^2-y^2}$  orbitals. The characteristic band degeneracy (at  $k_z = \pi$  in the original BZ) allows us to construct a simple four-band model with the band unfolding approach (Fig.2). We also estimate the interaction parameters and

found that the system is more correlated than the 1111 family of iron-based superconductors. Provided the superconductivity is mediated by spin fluctuations, the  $3d_{xz}$ -like band should play an essential role, and the gap function changes its sign between the Fermi surfaces around the  $\Gamma$  point.

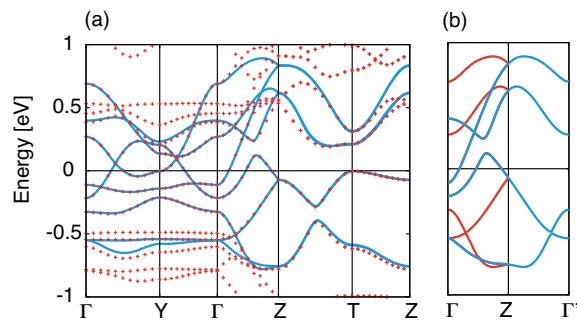


Figure 2: (a) Band dispersion of the effective two-orbital model. (b) Band dispersion in the extended Brillouin zone.

## References

- [1] H. Takahashi et al., *Nature Materials* **14**, (2015) 1008.
- [2] T. Yamauchi, Y. Hirata, Y. Ueda, and K. Ohgushi, *Phys. Rev. Lett.* **115**, (2015) 246402.
- [3] M-T. Suzuki, R. Arita and H. Ikeda, *Phys. Rev. B* **92**, (2015) 085116.
- [4] R. Arita, H. Ikeda, S. Sakai and M-T. Suzuki, *Phys. Rev. B* **92**, (2015) 054515.

# Numerical simulation of $^4\text{He}$ adsorbed on substrates

Yuichi MOTOYAMA

*Institute for Solid State Physics, University of Tokyo*  
*Kashiwa-no-ha, Kashiwa, Chiba 277-8581*

$^4\text{He}$  atoms adsorbed on a substrate such as graphite form a layer structure and a layer is an ideal two dimensional interacting bosonic system. Greywall and Busch [1] measured the heat capacity of the first layer of  $^4\text{He}$  atoms on a graphite and found that a single phase transition occurs at temperature  $T \simeq 1\text{K}$  below areal density  $\rho = 0.4\text{\AA}^{-2}$ . They concluded that KT and condensation (gas-liquid separation) transitions occur simultaneously as a single transition. However, they also pointed out that a problem still remains; at densities near the upper end of coexisting region, KT transition should occur at higher temperature than the condensation does.

For a preliminary simulation to examine this transition, I performed two grand-canonical path-integral Monte Carlo simulations with different initial condition of  $^4\text{He}$  atoms; one is vacuum phase and the other is commensurate solid phase (C 1/3 phase) with respect to the below carbons. Other simulation parameters are as following: The simulation cell is of  $44.28\text{\AA}(x) \times 42.61\text{\AA}(y) \times 9\text{\AA}(z)$ , the boundary condition is periodic along  $x$  and  $y$  direction, parallel to graphite surface, and is open along  $z$  direction. The imaginary time step  $d\tau$  is  $0.005\text{K}^{-1}$ . The potentials that a  $^4\text{He}$  atom feels from another  $^4\text{He}$  atom and the graphite are the Aziz potential [2] and the Carlos-Cole potential [3], respectively. Figure 1 shows the difference of areal density of the first layer of  $^4\text{He}$  between the two simulations. The average over 100,000 Monte Carlo steps after discarded 500,000 (1,000,000) steps is shown in the left (right) panel. From this figure, it is concluded

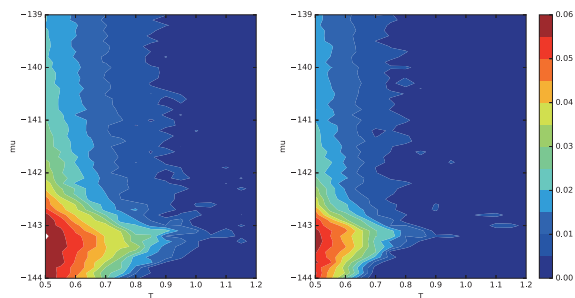


Figure 1: Difference of areal density of  $^4\text{He}$  on a graphite between two simulations with different initial condition; one is vacuum and the other is commensurate solid with respect to the carbon atoms of graphite. The numbers of discarded Monte Carlo steps are 500,000 for the left panel and 1,000,000 for the right.

that a line of first order phase transition exists at about  $\mu = -143.2\text{K}$  and ends at  $T \simeq 0.9\text{K}$ .

## References

- [1] D. S. Greywall and P. A. Busch, Phys. Rev. Lett. **67**, 3535 (1991).
- [2] R. A. Aziz, V. P. S. Nain, J. S. Carley, W. L. Taylor, and G. T. McConville, J. Chem. Phys. **70**, 4330 (1979).
- [3] W. E. Carlos and M. W. Cole, Surface Science **91**, 339 (1980).
- [4] I used ALPS/parapack library [5] for embarrassingly parallelization and job scheduling.
- [5] B. Bauer et al. (ALPS collaboration), J. Stat. Mech. P05001 (2011).

# Quantum Monte Carlo simulation and electronic state calculations in correlated electron systems

Takashi YANAGISAWA

*Electronics and Photonics Research Institute*

*National Institute of Advanced Industrial Science and Technology (AIST)*

*AIST Central 2, 1-1-1 Umezono, Tsukuba 305-8568*

High-temperature superconductors have been studied intensively since the discovery of high-temperature cuprates. The electron correlation between electrons is important because parent compounds without carriers are insulators. It is primarily important to clarify electronic states in the  $\text{CuO}_2$  plane contained in cuprate high-temperature superconductors. The mechanism of superconductivity has been investigated, but it remains unresolved. It is obvious that interaction with large energy scale is necessary and responsible for realization of high-temperature superconductivity. The Coulomb interaction has obviously a large characteristic energy scale and is a candidate of interaction that induces high-temperature superconductivity.

We have carried out numerical computations by using a Monte Carlo procedure to calculate expectation values of physical quantities. We performed parallel computing with 192 cores mainly on the system B.

The single-band Hubbard model is given by

$$H = \sum_{ij\sigma} t_{ij} c_{i\sigma}^\dagger c_{j\sigma} + U \sum_i n_{i\uparrow} n_{i\downarrow}, \quad (1)$$

where  $t_{ij}$  are transfer integrals and  $U$  is the on-site Coulomb energy. The transfer integral  $t_{ij}$  is non-zero  $t_{ij} = -t$  for nearest-neighbor pair  $\langle ij \rangle$  and  $t_{ij} = -t'$  for next-nearest neighbor  $\langle\langle ij \rangle\rangle$ . Otherwise  $t_{ij}$  vanishes. We denote the number of sites as  $N$  and the number of electrons as  $N_e$ . The energy unit is given by  $t$ .

The wave function should include correlation between electrons. The well-known Gutzwiller wave function is given by  $\psi_G = P_G \psi_0$  where  $P_G$  is the Gutzwiller operator defined by  $P_G = \prod_j (1 - (1 - g)n_{j\uparrow}n_{j\downarrow})$  with

the variational parameter  $g$  in the range of  $0 \leq g \leq 1$ . It is necessary to improve the Gutzwiller wave function because only the on-site correlation is considered in the Gutzwiller ansatz. The one way to improve the wave function is to take account of nearest-neighbor doublon-holon correlation:  $\psi_{d-h} = P_{d-h} P_G \psi_0$ . We can take into account inter-site correlations by multiplying  $P_J$  such as  $P_J P_{d-h} P_G \psi_0$ .

In the other way, we can take account of inter-site correlation by multiplying the kinetic operator to the Gutzwiller function in order to improve the wave function. A typical wave function of this type is written as[1]

$$\psi_\lambda \equiv \psi^{(2)} = e^{-\lambda K} P_G \psi_0, \quad (2)$$

where  $K$  is the kinetic term in the Hamiltonian:  $K = \sum_{ij\sigma} t_{ij} c_{i\sigma}^\dagger c_{j\sigma}$  and  $\lambda$  is a variational parameter to be optimized to lower the energy. This wave function is further improved by multiplying the Gutzwiller operator again:

$$\psi^{(3)} \equiv P_G \psi_\lambda = P_G e^{-\lambda K} P_G \psi_0. \quad (3)$$

The expectation values for these wave functions are evaluated by using the variational Monte Carlo method.

It is seen that the energy is not so improved only by multiplying the doublon-holon correlation factor  $P_{d-h}$  to the Gutzwiller function. The trial wave function  $P_{d-h} P_G \psi_0$  was used to develop the physics of Mott transition following the suggestion that the Mott transition occurs due to doublon-holon binding. We before examined the Mott transition with the wave function  $e^{-\lambda K} P_G \psi_0$ [4] because the variational energy by this wave function is much lower than that of the doublon-holon wave function.

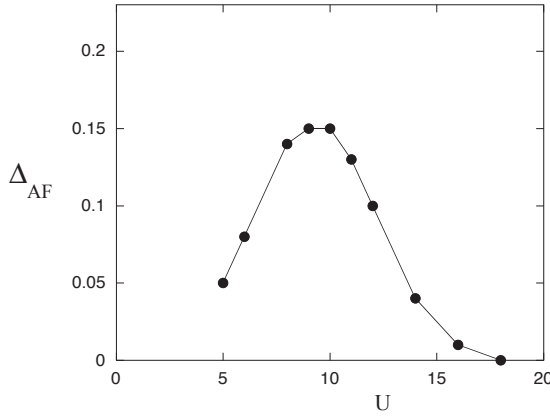


Figure 1: Antiferromagnetic order parameter  $\Delta_{AF}$  as a function of  $U$  in units of  $t$  on  $10 \times 10$  lattice. The number of electrons is  $N_e = 84$  and we set  $t' = -0.2t$ . We used the periodic boundary condition in both directions.

We show the antiferromagnetic (AF) order parameter  $\Delta_{AF}$  as a function of  $U$  in Fig.1[5]. This is a typical behavior of  $\Delta_{AF}$  and the AF energy gain  $\Delta E_{AF}$  also shows a similar behavior. The calculation was carried out, by employing the wave function  $\psi_\lambda$ , on a  $10 \times 10$  lattice. When  $U$  is small,  $\Delta_{AF}$  increases with the increase of  $U$  and has a maximum at  $U_m \simeq 8t - 10t$  that is of the order of the bandwidth. When  $U$  is larger than  $U_m$ , the  $\Delta_{AF}$  is decreased as  $U$  is increased. This indicates that AF correlation is suppressed for extremely large  $U$  and diminishes. In the region  $U > U_m$ , there is a competition between AF correlation and charge fluctuation; this means that we must have the AF energy gain or kinetic energy gain to lower the ground-state energy. The  $\Delta_{AF}$  is reduced gradually as  $U$  is increased ( $U > U_m$ ) since the energy gain  $\Delta E_{AF}$  is presumably proportional to the AF exchange coupling  $J \propto t^2/U$ . The AF correlation should be suppressed to get the kinetic energy gain for large  $U$ . Thus we have weak AF correlation in the strongly correlated region with  $U \geq U_m$ . This indicates that there is a large AF fluctuation in this region, brought about by charge fluctuation, where the charge fluctuation is driven by the kinetic operator  $K$  in the exponential factor  $\exp(-\lambda K)$ . This charge fluctuation is properly called the kinetic charge

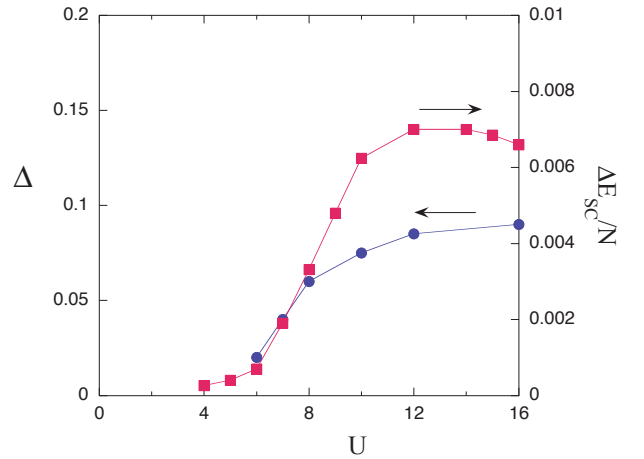


Figure 2: Superconducting order parameter  $\Delta$  and superconducting condensation energy  $\Delta E_{SC}$  per site as a function of  $U$  in units of  $t$  on  $10 \times 10$  lattice. The number of electrons is  $N_e = 84$  and  $t' = -0.2t$ . The boundary condition is periodic in one direction and antiperiodic in the other direction.

fluctuation.

It has turned out that there is large spin fluctuation being driven by kinetic charge fluctuation. We expect that a pairing interaction is inspired by this kind of large spin fluctuation. In fact, the optimized superconducting order parameter increases as  $U$  is increased and has a maximum at some  $U$  being greater than  $U_m$ . This is shown in Fig.2 where the superconducting order parameter  $\Delta$  and the condensation energy  $\Delta E_{SC}$  are shown as a function of  $U$ .  $\Delta E_{SC}$  has a maximum at  $U \sim 12t$ . This result was obtained by using the Gutzwiller-BCS function  $P_{N_e} P_G \psi_{BCS}$ . It indicates that the superconducting state becomes more stable in the strongly correlated region.

## References

- [1] T. Yanagisawa et al., J. Phys. Soc. Jpn. 67, 3867 (1998).
- [2] T. Yanagisawa and M. Miyazaki, EPL 107, 27004 (2014).
- [3] T. Yanagisawa and I. Hase, Physica C (2016).

## The correlation between the real space hoppings and $T_c$ in the iron-based superconductors

KAZUHIKO KUROKI

*Department of Physics, Osaka University*

*1-1 Machikaneyama, Toyonaka, Osaka, 560-0043, Japan*

### HYDROGEN DOPED IRON-BASED SUPERCONDUCTORS

In the hydrogen doped 1111 iron pnictides  $\text{LaFeAsO}_{1-x}\text{H}_x$ , electron doping rate can exceed 50 percent, and the  $T_c$  against the doping rate  $x$  exhibits a double dome structure, where the second dome with higher doping concentration has the higher  $T_c$ [1]. In a rigid band picture, such a large amount of electron doping would wipe out the hole Fermi surfaces, so that the Fermi surface nesting would no longer be good in the higher  $T_c$  second dome.

### EVOLUTION OF THE FERMI SURFACE

First principles band calculation that takes into account the band structure variation with chemical substitution reveals that the band structure rapidly changes with doping, and the rigid band picture is not valid[2–4]. In momentum space, the  $d_{xz/yz}$  hole Fermi surfaces around (0,0) shrink monotonically and are eventually lost with sufficient electron doping, and in turn an electron Fermi surface appears. On the other hand, an interesting point is that the  $d_{xy}$  hole Fermi surface around  $(\pi, \pi)$  is barely changed with the doping rate  $x$ , which is clearly a non-rigid band feature.

### REAL SPACE HOPPINGS

Analyzing the tightbinding model derived based on the first principles band and exploiting the maximally localized Wannier orbitals, it is revealed that the insensitivity of the  $d_{xy}$  Fermi surface is due to a rapid decrease of  $t_1$  within the  $d_{xy}$  orbital upon increasing  $x$ , which pushes up the  $d_{xy}$  band top at  $(\pi, \pi)$ , so that it follows the increase of the Fermi level. It should be noted that reduction of  $t_1$  is largely due to the increase of the positive charge within the blocking layer by O(2-)→H(1-) substitution, which in turn reduces the As 4*p* electronic level and leads to the suppression of the indirect component of  $t_1$ [4]. We have found that a similar situation can occur when pressure is applied to some of the iron-based superconductors.

### CORRELATION BETWEEN HOPPINGS, SPIN FLUCTUATION AND SUPERCONDUCTIVITY

The  $d_{xy}$  hole Fermi surface remains even at large electron doping rate, while the  $d_{xz/yz}$  hole Fermi surfaces are lost, so that the importance of the  $d_{xy}$  orbital increases with doping. Our fluctuation exchange study of these non-rigid band models show that the spin fluctuation and the  $s \pm$  pairing are both enhanced in this largely doped regime, exhibiting a double dome feature of the superconducting  $T_c$  as a function of doping. Moreover, the two domes are merged into a single dome when the Pn-Fe-Pn bond angle is reduced (a change that takes place when the rare earth is varied as La→Ce→Sm→Gd), in agreement with the experimental observations. Although the  $d_{xy}$  hole Fermi surface remains unchanged in the highly doped regime, the Fermi surface nesting in its original sense is monotonically degraded because the volume of the electron Fermi surfaces increases. Hence, the origin of the second dome in  $\text{LaFeAsO}_{1-x}\text{H}_x$  cannot be attributed to a good Fermi surface nesting.

$s \pm$  pairing is a next nearest neighbor pairing, which is favored by the relation between nearest and next nearest neighbor antiferromagnetic interactions  $J_2 > J_1$ , corresponding to  $t_2 > t_1$ . In fact, as mentioned above,  $t_2$  dominating over  $t_1$  is what is happening in the second  $T_c$  dome regime. Hence, intuitively,  $t_2 > t_1$  can be considered as the origin of the  $T_c$  enhancement in the largely doped regime. To be precise, however, the fluctuation exchange approximation is a weak coupling method based on the itinerant spin model, so using the  $J_1 - J_2$  term of the localized spin model is not conceptually correct. In reality, the entire  $d_{xy}$  portion of the band structure is strongly modified in a manner that it favors the second nearest neighbor pairing. To see in more detail the effect of this modified band structure, we have further analyzed the correlation between the real space hoppings and the energy dependence of the spin fluctuation by calculating the imaginary part of the dynamical spin susceptibility. We find that as the Fermi surface nesting is degraded upon electron doping, the low energy spin fluctuation is suppressed, and the weight is shifted in the high energy regime. This is natural

since the Fermi surface nesting in its original sense should enhance zero energy spin fluctuation. The enhancement of  $s\pm$  spin fluctuation in the heavily electron doped regime can then be attributed to the enhancement of finite energy spin fluctuation. It is important to note that this behavior is peculiar to systems with disconnected Fermi surfaces, where the nesting vector itself is barely varied even when the degree of the nesting is degraded.

- 
- [1] S. Iimura, S. Matsuishi, H. Sato, T. Hanna, Y. Muraba, S.W. Kim, J. E. Kim, M. Takata and H. Hosono, Nat. Commun. 3, 943 (2012).
  - [2] S. Iimura, S. Matsuishi, M. Miyakawa, T. Taniguchi, K. Suzuki, H. Usui, K. Kuroki, R. Kajimoto, M. Nakamura, Y. Inamura, K. Ikeuchi, S. Ji, and H. Hosono, Phys. Rev. B, 060501(R) (2013).
  - [3] K. Suzuki, H. Usui, K. Kuroki, S. Iimura, Y. Sato, S. Matsuishi, and H. Hosono, J. Phys. Soc. Jpn. 82, 083702 (2013).
  - [4] K. Suzuki, H. Usui, S. Iimura, Y. Sato, S. Matsuishi, H. Hosono, and K. Kuroki Phys. Rev. Lett. 113, 027002 (2014)

# Monte Carlo Study of Itinerant and Localized Chiral Helimagnets

Shintaro HOSHINO

*Department of Basic Science, The University of Tokyo, Meguro, Tokyo 153-8902, Japan*

Chiral magnets with the asymmetric Dzyaloshinskii-Moriya interaction show intriguing behaviors beyond simple magnetic structures such as ferro- and antiferromagnetism. In  $\text{CrNb}_3\text{S}_6$ , the helical magnetic structure is realized at zero field. With increasing external field it changes into the chiral soliton lattice where the quasi-local magnetic kinks are aligned periodically [1, 2, 3]. The localized spins of the Cr ions are responsible for the magnetism and are coupled with each other through the Ruderman-Kittel-Kasuya-Yoshida interaction mediated by conduction electrons.

Since the characteristic length scale for the magnetic structure is much larger than the lattice constant in  $\text{CrNb}_3\text{S}_6$ , the low-energy behaviors are not sensitive to the fine structure of the system. Hence we choose the simplest classical spin model that can describe helical magnet and chiral soliton lattice structure. The explicit form of Hamiltonian is written as

$$\mathcal{H} = \sum_{ij} (J_{ij} \mathbf{S}_i \cdot \mathbf{S}_j + \mathbf{D}_{ij} \cdot \mathbf{S}_i \times \mathbf{S}_j) - \sum_i \mathbf{H} \cdot \mathbf{S}_i \quad (1)$$

The vector  $\mathbf{D}_{ij}$  is along the helical axis. The interaction parameter  $J_{ij}$  for the helical axis is much smaller than the one perpendicular. This strong anisotropy originates from quasi-two-dimensional electronic structure.

We have analyzed this model by using the mean-field theory [4]. Under the external magnetic field, the system has many metastable states characterized by the winding number. More specifically, if we use the initial condi-

tion with the form

$$\langle \mathbf{S}_i \rangle = S(\cos(2\pi i_{\parallel} w / N_{\parallel}), \sin(2\pi i_{\parallel} w / N_{\parallel}), 0) \quad (2)$$

we obtain the different solution for each winding number  $w$ . Here  $i_{\parallel}$  and  $N$  are the site index and the number of sites, respectively, along the helical axis. At each parameter we calculate solutions for all the possible  $w$ , and determine the most appropriate solution by comparing the value of free energy. The numerical computation has been efficiently performed by parallelization of the calculations at each  $w$  using supercomputer in ISSP. The realistic Dzyaloshinskii-Moriya interaction parameter for  $\text{CrNb}_3\text{S}_6$  is given by  $D = 0.16J$  which means the long periodicity of the helical structure. Hence our mean-field calculation requires a large system size. We take typically  $N = 4000$  for the numerical simulation.

As one of the exemplary results of our study, we shown in Fig. 1 the free energy profile near the transition temperature under magnetic field [4]. The free energy has a double-minimum structure and thus we have identified first-order transition character. This behavior

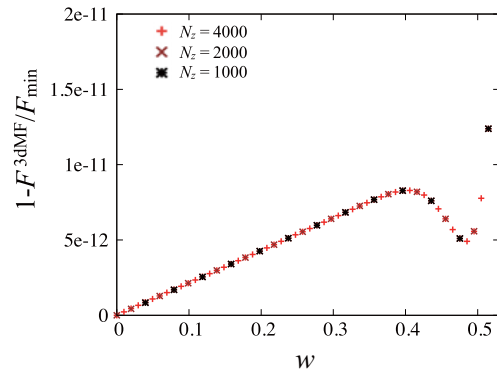


Figure 1: Free energy profile as a function of winding number  $w$ . The size ( $N_z$ ) dependence is shown.

appears at finite temperatures and finite external fields, and is not observed in the zero-temperature nor zero-field limit. The change of the order of phase transition along the phase boundary was also discussed recently by two groups [5, 6]. The systematic studies is necessary to clarify the nature of phase transitions.

## References

- [1] I. E. Dzyaloshinskii, *Sov. Phys. JETP* **20**, 665 (1965).
- [2] T. Moriya and T. Miyadai, *Solid State Commun.* **42**, 209 (1982).
- [3] J. Kishine, K. Inoue, and Y. Yoshida, *Prog. Theor. Phys. Suppl.* **159**, 82 (2005).
- [4] M. Shinozaki, S. Hoshino, Y. Masaki, J. Kishine and Y. Kato, arXiv1512.00235 (2015).
- [5] Y. Nishikawa, K. Hukushima, arXiv:1603.04200 (2016).
- [6] V. Laliena, J. Campo, Y. Kousaka, and K. Inoue, arXiv:1603.06362 (2016).

# Novel Charge Dynamics in Correlated Electron Systems

Sumio ISHIHARA

*Department of Physics, Tohoku University*

*Sendai 980-8578*

Electronic charge degree of freedom plays essential roles in dielectric, transport and optical properties in correlated electron systems, such as transition-metal oxides, and low dimensional organic salts. In the projects (H27-Ba-0014 and H27-Bb-0028), we have studied numerically the novel charge dynamics in correlated systems with multi degree of freedom. The following are the list of the obtained results.

1) Transient dynamics of the frustrated interacting charge systems coupled with the lattice degree of freedom are examined numerically. Real-time dynamics in the triangular-lattice spinless fermion model with lattice vibration are analyzed by the exact diagonalization method based on the Lanczos algorithm combined with the equation of motion. A photoinduced phase transition from the horizontal stripe-type charge order to the 3-fold charge order occurs through a characteristic intermediate time domain (Fig. 1). By analyzing the time evolution, we find that these characteristic dynamics are seen when the electron and lattice sectors are not complementary to each other but show cooperative time evolutions. [1].

2) Charge dynamics in a frustrated system are studied in wide ranges of energy, momentum, and temperature. As a typical frustrated charge system, we adopt an interacting spinless fermion model on a paired-triangular lattice which was proposed as an electronic model of the layered iron oxide  $\text{LuFe}_2\text{O}_4$  a candidate

material for the electronic ferroelectricity. In particular, we focus on the charge dynamics in the three-fold charge order and the two-fold charge order. The optical conductivity spectra in the three-fold charge order show multiple components and their low-energy weights survive even below the charge order temperature. These are related to the stability of the three-fold charge order and are in sharp contrast to the spectra in the two-fold charge order. The change in the dynamical charge correlation below the charge ordering temperature is weakly momentum-dependent in the three-fold charge order, and an abrupt reduction is observed in the two-fold charge order. These results are attributable to the charge frustration effects, and explain some aspects of the results of recent optical and resonant inelastic x-ray scattering experiments [2, 3].

3) A possible way to realize the magnetoelectric (ME) effect in the dimer-type organic molecular solids is studied. We show a symmetrical considerations in a simple one-dimensional model (Fig. 2). Next, we have carried out the numerical calculations in a two-dimensional lattice model for the  $\kappa$ -(BEDT-TTF) type organic molecular solids. We find that the linear ME effect emerges in a long-range ordered state of spins and electric dipoles owing to the electronic degree of freedom inside the molecular dimers. The essence of this ME effect is attributed to a ferroic order of the spin-charge composite object. The ME effect is also realized in the spin and charge disordered

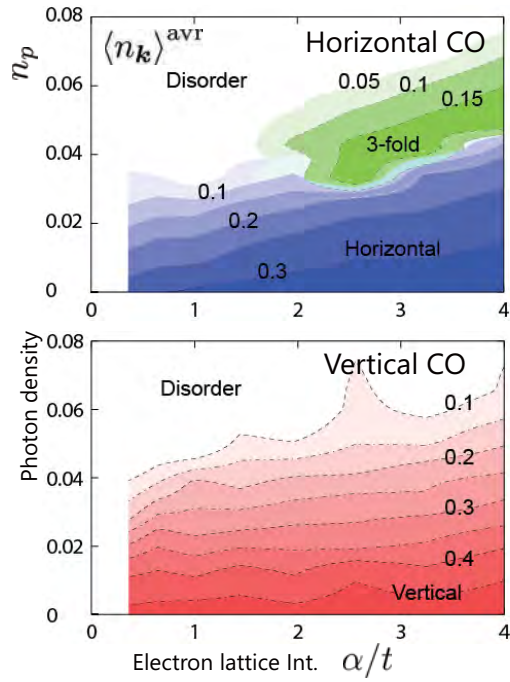


Figure 1: Phase diagrams in the excited states for the horizontal and vertical charge ordered states. Horizontal and vertical axes represent the electron lattice interaction and the photon density, respectively. Colors represent amplitudes of the order parameters. [1].

state, in which the spin-charge composite order emerges. [4]

The present researches has been collaborated with J. Nasu (Tokyo Institute of Technology), M. Naka (Tohoku University), H. Hashimoto (Tohoku University), H. Matsueda (Sendai National College of Technology) and H. Seo (RIKEN, CEMS). Some parts of the computation in the present works has been done using the facilities of the Supercomputer Center, the Institute for Solid State Physics, the University of Tokyo.

## References

- [1] H. Hashimoto, H. Matsueda, H. Seo, and S. Ishihara, *J. Phys. Soc. Jpn.* **84**, (2015) 113702.

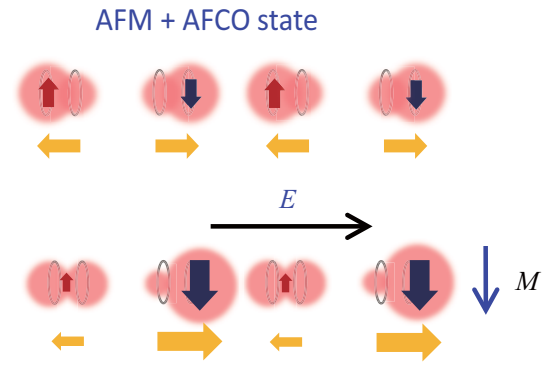


Figure 2: (top): A schematic view of the anti-ferromagnetic and antiferroelectric charge ordered state in the dimer-Mott insulating system. (bottom): Magnetolectric effect in the system. [4].

- [2] M. Naka and S. Ishihara, *J. Phys. Soc. Jpn.* **84**, (2015) 023703.

- [3] M. Yoshida, K. Ishii, M. Naka, S. Ishihara, I. Jarrige, K. Ikeuchi, Y. Murakami, K. Kudo, Y. Koike, T. Nagata, Y. Fukada, N. Ikeda and J. Mizuki, *Scientific Report* **6**, (2015) 23611.

- [4] M. Naka and S. Ishihara, *Scientific Report* **6**, (2015) 20781.

# Magnetic properties in the Hubbard model on the Honeycomb Lattice by variational cluster approximation

Atsushi Yamada

*Department of Physics, Chiba University  
Chiba 263-8522, Japan, Chiba 277-8581*

A spin liquid state, which is a purely non-magnetic Mott insulator without spontaneously broken spatial or spin symmetry, has attracted a lot of interest. This state is realized in geometrically frustrated systems like the charge organic transfer salts  $\kappa$ -(BEDT-TTF)<sub>2</sub>X[1] and Cs<sub>2</sub>CuCl<sub>4</sub>. [2] A simple theoretical model of these compounds is the Hubbard model on the an-isotropic triangular lattice, and spin liquid state is in fact found in this model. [3] A spin liquid could arise also in the intermediate coupling region of strongly correlated systems between a semi-metal and ordered state, because in this case a correlation-driven insulating gap might open before the system becomes ordered. This possibility might be realized in the half-filled Hubbard model on the honeycomb lattice.

We have studied the magnetic and metal-to-insulator transitions by variational cluster approximation using 10-site cluster as a reference system. Parts of numerical calculations were done using the computer facilities of the ISSP. We found that  $U_{AF} = 2.7$  and  $U_{MI} = 3.0$ . This result also rules out the existence of the spin liquid in this model. Both the magnetic and non-magnetic metal-to-insulator transitions are of the second order. Our results agree with recent large scale Quantum Monte Carlo simulations. [4]

We plan to continue this study using larger reference cluster to see the cluster size dependence of the results. [5]

## References

- [1] Y. Shimizu, K. Miyagawa, K. Kanoda, M. Maesato, and G. Saito, Phys. Rev. Lett. **91**, 107001 (2003); Y. Kurosaki, Y. Shimizu, K. Miyagawa, K. Kanoda, and G. Saito, Phys. Rev. Lett. **95**, 177001 (2005).
- [2] R. Coldea, D.A. Tennant, A.M. Tsvelik, and Z. Tylczynski, Phys. Rev. Lett. **86**, 1335 (2001); R. Coldea, D.A. Tennant, and Z. Tylczynski, Phys. Rev. Lett. **68**, 134424 (2003).
- [3] T. Yoshioka, A. Koga, and N. Kawakami, Phys. Rev. Lett. **103**, 036401 (2009); P. Sahebsara and D. Sénéchal, Phys. Rev. Lett. **100**, 136402 (2008); L.F. Tocchio, H. Feldner, F. Becca, R. Valentí, and C. Gros, Phys. Rev. B **87**, 035143 (2013); A. Yamada, Phys. Rev. B **89**, 195108 (2014); L.F. Tocchio, C. Gros, R. Valentí, F. Becca, Phys. Rev. B **89**, 235107 (2014); A. Yamada, Phys. Rev. B **90**, 235138 (2014).
- [4] S. Sorella, Y. Otsuka, and S. Yunoki, Sci. Rep. **2**, 992 (2012); F. F. Assaad and I. F. Herbut, Phys. Rev. X **3**, 031010 (2013); F. Parisen Toldin, M. Hohenadler, F. F. Assaad, and I. F. Herbut, Phys. Rev. B **91**, 165108 (2015).
- [5] A. Yamada, in preparation.

# Optical conductivity near antiferromagnetic transition in the square-lattice Hubbard model

Toshihiro SATO

*Computational Condensed Matter Physics Laboratory, RIKEN  
Wako, Saitama 351-0198, Japan*

A cluster dynamical mean field theory (CDMFT) [1] has advanced our understanding of electronic properties in strongly correlated electronic systems described by the Hubbard model such as metal-insulator Mott transition, pseudogap state, and superconductivity. Recently, the focus has shifted to move onto transport properties. Optical conductivity is one of the most fundamental transport coefficient and provides useful information on charge dynamics, particularly effective mass and transport scattering process as well as electric structure.

The main purpose of this study is to derive a new formula of optical conductivity on the antiferromagnetic phase based on our previous one for the paramagnetic phase [2]. To take into account both strong short-range electronic correlations and magnetic fluctuations, we employ the CDMFT using a four-site square cluster and calculate optical conductivity with including the vertex corrections near the antiferromagnetic transition in a square-lattice Hubbard model at half filling,  $H = -t \sum_{\langle i,j \rangle, \sigma} c_{i\sigma}^\dagger c_{j\sigma} + U \sum_i n_{i\uparrow} n_{i\downarrow} - \mu \sum_{i,\sigma} n_{i\sigma}$ . Here,  $t$  is the nearest-neighbor hopping amplitude,  $U$  is the on-site Coulomb repulsion and  $\mu$  is the chemical potential.  $c_{i\sigma}$  is the electron annihilation operator at site  $i$  with spin  $\sigma$  and  $n_{i\sigma} = c_{i\sigma}^\dagger c_{i\sigma}$ . The numerical solver is the continuous-time quantum Monte Carlo method based on the strong coupling expansion [3]. This is performed by the large-scale numerical computations using facilities at Supercomputer Center in ISSP.

We calculate temperature-dependence of optical conductivity  $\sigma(\omega)$  at  $U = 6.5t$  fixed and investigate the effects of the vertex corrections. Figure 1 presents the contributions of vertex

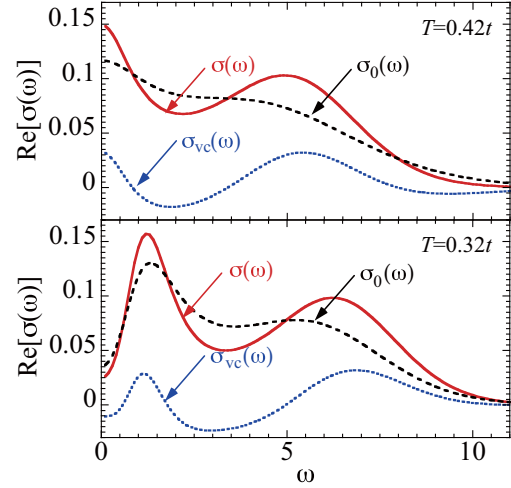


Figure 1: Effects of vertex corrections on optical conductivity  $\sigma(\omega)$  in the paramagnetic phase ( $T = 0.42t$ ) and the antiferromagnetic phase ( $T = 0.32t$ ).  $\sigma(\omega)$  is the result with vertex corrections,  $\sigma_0(\omega)$  is the result without vertex corrections, and the contribution of vertex corrections is  $\sigma_{vc}(\omega)$ .

corrections:  $\sigma(\omega)$  is the result with vertex corrections,  $\sigma_0(\omega)$  is the result without vertex corrections, and the contribution of vertex corrections is  $\sigma_{vc}(\omega)$ . The most important finding is that vertex corrections change various important details in temperature and frequency dependence of conductivity. In the paramagnetic phase, the vertex corrections enhance both the Drude peak and the broad incoherent peak related to the Hubbard band and the two peaks become sharper. In the antiferromagnetic phase, the dip of  $\sigma(\omega)$  at  $\omega = 0$  is suppressed by the vertex corrections, in addition to the sharply enhancement of the low-energy peak around  $\omega = 1$ . Moreover, we demonstrate that in a temperature region just above the

antiferromagnetic transition temperature with including the vertex corrections, dc conductivity shows an insulating behavior, whereas the Drude peak is stable. We also investigate the momentum dependence of the vertex function and find that there exists very different fluctuations in the vertex corrections between quasiparticles at different positions in the Brillouin zone both in the paramagnetic and antiferromagnetic phases [4].

This work is done in collaboration with Prof. Hirokazu Tsunetsugu (ISSP, The University of Tokyo).

## References

- [1] G. Kotliar, S. Y. Savrasov, G. Pálsson, and G. Biroli: Phys. Rev. Lett. **87** (2001) 186401.
- [2] T. Sato, K. Hattori, and H. Tsunetsugu: Phys. Rev. B **86** (2012) 235137.
- [3] P. Werner, A. Comanac, L. de i Ç Medici, M. Troyer, and A. J. Millis: Phys. Rev. Lett. **97** (2006) 076405.
- [4] T. Sato and H. Tsunetsugu: submitted to Phys. Rev. B.

# Research of Kondo effect in $f^7$ -electron systems by numerical renormalization group method

Takashi HOTTA

*Department of Physics, Tokyo Metropolitan University  
1-1 Minami-Osawa, Hachioji, Tokyo 192-0397*

In order to promote our basic understanding of the Kondo behavior recently observed in europium compounds [1, 2, 3, 4], we analyze an impurity Anderson model with seven  $f$  electrons at an impurity site by employing a numerical renormalization group method [5].

The model is given by

$$\begin{aligned}
H = & \sum_{\mathbf{k}, m, \sigma} \varepsilon_{\mathbf{k}m} c_{\mathbf{k}m\sigma}^\dagger c_{\mathbf{k}m\sigma} \\
& + \sum_{\mathbf{k}, m, \sigma} (V_m c_{\mathbf{k}m\sigma}^\dagger f_{m\sigma} + \text{h.c.}) \\
& + \lambda \sum_{m, \sigma, m', \sigma'} \zeta_{m, \sigma; m', \sigma'} f_{m\sigma}^\dagger f_{m'\sigma'} \\
& + \sum_{m, m', \sigma} B_{m, m'} f_{m\sigma}^\dagger f_{m'\sigma} \\
& + \sum_{\substack{m_1 \sim m_4 \\ \sigma, \sigma'}} I_{m_1 m_2, m_3 m_4} f_{m_1 \sigma}^\dagger f_{m_2 \sigma'}^\dagger f_{m_3 \sigma'} f_{m_4 \sigma},
\end{aligned} \tag{1}$$

where  $\varepsilon_{\mathbf{k}m}$  is the dispersion of conduction electron with the  $z$ -component  $m$  of angular momentum  $\ell = 3$ ,  $c_{\mathbf{k}m\sigma}$  is an annihilation operator of conduction electron with momentum  $\mathbf{k}$ , angular momentum  $m$ , and spin  $\sigma$ ,  $\sigma = +1$  ( $-1$ ) for up (down) spin,  $f_{m\sigma}$  denotes the annihilation operator for local  $f$  electron,  $V_m$  is the hybridization between conduction and localized electrons,  $I_{m_1 m_2, m_3 m_4}$  indicates the Coulomb interaction,  $\lambda$  is the spin-orbit coupling, and  $B_{m, m'}$  denotes the crystalline electric field (CEF) potential.

The Coulomb interaction  $I$  is known to be expressed by the Slater-Condon parameters,  $F^0$ ,  $F^2$ ,  $F^4$ , and  $F^6$ . Although these should be determined for the material from the experi-

mental results, here we assume the ratio among the Slater-Condon parameters as  $F^0 = 10U$ ,  $F^2 = 5U$ ,  $F^4 = 3U$ , and  $F^6 = U$ , where  $U$  is the Hund's rule interaction among  $f$  orbitals. Each matrix element of  $\zeta$  for the spin-orbit coupling is given by  $\zeta_{m, \sigma; m, \sigma} = m\sigma/2$ ,  $\zeta_{m+\sigma, -\sigma; m, \sigma} = \sqrt{\ell(\ell+1) - m(m+\sigma)}/2$ , and zero for other cases. The CEF potentials for  $f$  electrons from the ligand ions is given in the table of Hutchings for  $\ell = 3$ . For cubic structure with  $O_h$  symmetry,  $B_{m, m'}$  is expressed by a couple of CEF parameters,  $B_4^0$  and  $B_6^0$ , which are given by  $B_4^0 = Wx/F(4)$  and  $B_6^0 = W(1 - |x|)/F(6)$ . Here  $x$  indicates the CEF scheme for the  $O_h$  point group, while  $W$  determines the energy scale for the CEF potentials. We choose  $F(4) = 15$  and  $F(6) = 180$  for  $\ell = 3$ .

Here we consider a single  $a_u$  conduction band, since the local  $a_u$  state is non-degenerate even under a high-symmetry ligand field such as the cubic CEF potential. Note that the local  $a_u$  state is described as  $(f_{m=2, \sigma}^\dagger - f_{m=-2, \sigma}^\dagger)|0\rangle/\sqrt{2}$ , where  $|0\rangle$  denotes the vacuum. Thus,  $V_m$  is given by  $V_{m=2} = -V_{m=-2} = V$  and is zero for other components. The energy unit is half of the  $a_u$  conduction bandwidth, which is set as 1 eV throughout this paper, as mentioned above.

For the diagonalization of the impurity Anderson model, we employ a numerical renormalization group (NRG) method [6, 7], in which we logarithmically discretize the momentum space so as to include efficiently the

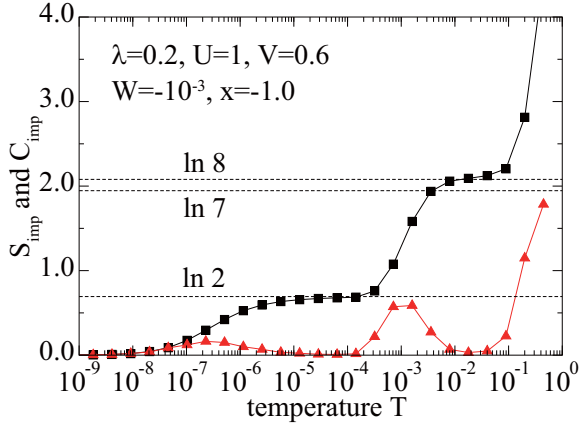


Figure 1: Entropy  $S_{\text{imp}}$  (solid squares) and specific heat  $C_{\text{imp}}$  (solid triangles) for  $\lambda = 0.2$ ,  $U = 1$ ,  $W = -10^{-3}$ ,  $x = -1.0$ , and  $V = 0.6$ .

conduction electrons near the Fermi energy. The conduction electron states are characterized by “shell” labeled by  $N$  and the shell of  $N = 0$  denotes an impurity site described by the local Hamiltonian.

For  $\lambda = 0$ , we observe underscreening Kondo behavior for appropriate values of  $V$ , characterized by an entropy change from  $\ln 8$  to  $\ln 7$ , in which one of the seven  $f$  electrons is screened by conduction electrons. When  $\lambda$  is increased, we obtain two types of behavior depending on the value of  $V$ . For large  $V$ , we find an entropy release of  $\ln 7$  at low temperatures, determined by the level splitting energy due to the hybridization. For small  $V$ , we also observe an entropy change from  $\ln 8$  to  $\ln 2$  by the level splitting due to the hybridization, but at low temperatures,  $\ln 2$  entropy is found to be released, leading to the Kondo effect. We emphasize that the Kondo behavior for small  $V$  is observed for realistic values of  $\lambda$  on the order of 0.1 eV.

In Fig. 1, we depict the temperature dependence of the entropy  $S_{\text{imp}}$  and specific heat  $C_{\text{imp}}$  for  $\lambda = 0.2$ ,  $U = 1$ ,  $W = -10^{-3}$ ,  $x = -1.0$ , and  $V = 0.6$ . We find a plateau of  $\ln 8$  around at  $T = 10^{-2}$  originating from the local octet of  $J = 7/2$ . For the case of  $\lambda = 0$ , only one electron spin is screened by

one conduction band, leading to the entropy changing from  $\ln 8$  to  $\ln 7$ , but in the present case with  $\lambda = 0.2$ , first we find that the entropy changes from  $\ln 8$  to  $\ln 2$  by the level splitting due to the hybridization with conduction electrons. Then, the entropy of  $\ln 2$  is eventually released at around  $T = 10^{-7}$ , leading to the Kondo temperature  $T_K$ . The behavior of the entropy and specific heat is essentially the same as those without the CEF potentials. This is not surprising, since the level splitting due to the hybridization plays the same role as that in the case of the CEF potentials.

## References

- [1] A. Mitsuda, S. Hamano, N. Araoka, H. Yayama, and H. Wada, *J. Phys. Soc. Jpn.* **81**, 023709 (2012).
- [2] Y. Hiranaka, A. Nakamura, M. Hedo, T. Takeuchi, A. Mori, Y. Hirose, K. Mitamura, K. Sugiyama, M. Hagiwara, T. Nakama, and Y. Ōnuki, *J. Phys. Soc. Jpn.* **82**, 083708 (2013).
- [3] A. Nakamura, T. Takeuchi, H. Harima, M. Hedo, T. Nakama, and Y. Ōnuki, *J. Phys. Soc. Jpn.* **83**, 053708 (2014).
- [4] A. Nakamura, T. Okazaki, M. Nakashima, Y. Amako, K. Matsubayashi, Y. Uwatoko, S. Kayama, T. Kagayama, K. Shimizu, T. Uejo, H. Akamine, M. Hedo, T. Nakama, Y. Ōnuki, and H. Shiba, *J. Phys. Soc. Jpn.* **84**, 053701 (2015).
- [5] T. Hotta, *J. Phys. Soc. Jpn.* **84**, 114707 (2015).
- [6] K. G. Wilson, *Rev. Mod. Phys.* **47**, 773 (1975).
- [7] H. R. Krishna-murthy, J. W. Wilkins, and K. G. Wilson, *Phys. Rev. B* **21**, 1003 (1980).

# General formalism for the anomalous-Hall or spin-Hall effects of interacting multiorbital metals

Naoya ARAKAWA

*Center for Emergent Matter Science, RIKEN*

*Wako, Saitama 351-0198*

Theoretical research about transport phenomena still need further development. One of the well known transport phenomena is the usual-Hall effect. The important development for the usual-Hall effect was obtained in the theoretical research [1] of a single-orbital Hubbard model on a square lattice: in this model near an antiferromagnetic quantum-critical point, the Hall coefficient showed the Curie-Weiss-like temperature dependence due to the strong antiferromagnetic spin fluctuation. This research showed the importance of the electron-electron interaction in the usual-Hall effect in a strongly correlated metal. Although the electron-electron interaction may be important even in another Hall effect such as the anomalous-Hall effect or the spin-Hall effect, our understanding of its effects is less developed than that for the usual-Hall effect.

About the effects of the electron-electron interaction in the anomalous-Hall or spin-Hall effect in metals, we have two important issues. One is about the roles of the Fermi-surface term and Fermi-sea term of the anomalous-Hall or spin-Hall conductivity in the presence of the electron-electron interaction. The theoretical research [2] neglecting the electron-electron interaction showed that the anomalous-Hall or spin-Hall conductivity at  $T = 0\text{K}$  without impurities was given by part of the Fermi-sea term, the Berry-curvature term, which was proportional to the Fermi distribution function, and that with increasing the nonmagnetic impurity concentra-

tion the dominant term of the anomalous-Hall or spin-Hall conductivity changed from the Berry-curvature term to the Fermi-surface term, which was proportional to the energy derivative of the Fermi distribution function. The other issue is about the spin-Colomb drag [3]. If the electron-electron interaction causes the scattering between different-spin electrons with finite momentum transfer in the presence of the onsite spin-orbit coupling, the total momentum of spin-up or spin-down electrons is not separately (but totally) conserved. This violation of the conservation law causes a characteristic friction of the spin current, the spin-Coulomb drag. Although the spin-Coulomb drag may affect the spin-Hall effect in metals and the effects may result in a characteristic property of the spin transports, the effects have not studied yet.

To develop our understanding of the electron-electron interaction in the anomalous-Hall and spin-Hall effects in metals, I construct the general formalism by using the linear-response theory with the approximations appropriate for metals, and clarify a new mechanism of the temperature dependence of the anomalous-Hall or spin-Hall conductivity at high or intermediate temperature even without impurities and the existence of the correction term of the spin-Hall conductivity due to the spin-Coulomb drag [4]. After deriving the exact expression of the anomalous-Hall or spin-Hall conductivity for a multiorbital Hubbard model with the onsite spin-

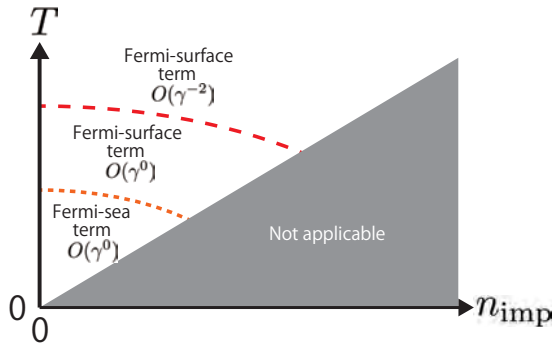


Figure 1: Schematic diagram about the dominant term and damping dependence of the anomalous-Hall or spin-Hall conductivity.

orbit coupling and the onsite weak-scattering potential of nonmagnetic impurities, I derive an approximate expression in Éliashberg's approximation, which is often used for the resistivity and the Hall coefficient in metals in the presence of the electron-electron interaction [5], and show that this approximation is applicable in the high-temperature and intermediate-temperature region in Fig. 1. As the result, I find that the dominant term of the anomalous-Hall or spin-Hall conductivity is the Fermi-surface term, resulting in the temperature dependence in the high-temperature region in Fig. 1 due to the dependence on the interaction-induced quasiparticle damping and the spin-Coulomb-drag-induced correction of the spin-Hall conductivity. Then, I construct an approximation beyond Éliashberg's approximation in order to describe the anomalous-Hall and spin-Hall effects in the low-temperature region of Fig. 1, and find that in this region the Fermi-sea term becomes dominant. In contrast to the Fermi-surface term, the Fermi-sea term is independent of the quasiparticle damping and is not affected by the spin-Coulomb drag.

The above theoretical research is the first step towards our thoroughly understanding of the electron-electron interaction in the anomalous-Hall or spin-Hall effect in metals. In particular, by combining the general formalism with the first-principle calculation, we can

analyze the anomalous-Hall or spin-Hall effect in metals in a realistic way.

## References

- [1] H. Kontani *et al.*: Phys. Rev. B **59** (1999) 14723.
- [2] H. Kontani *et al.*: Phys. Rev. B **75** (2007) 184416; H. Kontani *et al.*: Phys. Rev. B **77** (2008) 165117.
- [3] E. M. Hankiewicz and G. Vignale: J.Phys.:Condens.Matter **21** (2009) 253202.
- [4] N. Arakawa: arXiv:1510.03988.
- [5] N. Arakawa: arXiv:1505.05274.

# Charge-density wave and exciton condensation induced by Coulomb interaction and electron-lattice interaction

Hiroshi WATANABE

*RIKEN CEMS*

*2-1, Hirosawa, Wako-shi, Saitama 351-0198*

The charge-density wave (CDW) is widely observed in low-dimensional solids and has been extensively studied for a long time. Transition metal dichalcogenides (TMDC)  $\text{MX}_2$  ( $M$  = transition metal,  $X$  = S, Se, Te) are one of the typical CDW materials with a layered triangular lattice structure.  $1T$ - $\text{TiSe}_2$  shows commensurate  $2 \times 2 \times 2$  CDW below  $T_c=200\text{K}$  and also shows superconductivity (SC) by applying pressure or intercalation of Cu atoms. The origin of the CDW and SC is still controversial and two different mechanism are proposed: exciton condensation and band Jahn-Teller effect. Although the former is originated from the Coulomb interaction and the latter is originated from the electron-lattice interaction, they are not separable and closely related with each other.

In this project, we have studied the two-band Hubbard model in a two-dimensional triangular lattice including Coulomb and electron-lattice interactions to clarify the mechanism of CDW and possibility of exciton condensation in  $1T$ - $\text{TiSe}_2$  [1]. The ground state property is investigated by variational Monte Carlo (VMC) method. The Gutzwiller-Jastrow type wave function is used for electronic part and the Gaussian type wave function is used for lattice part of the VMC trial function. The system sizes for calculation are from  $12 \times 12 \times 2$  to  $24 \times 24 \times 2$ .

We have shown that the Coulomb and electron-lattice interactions cooperately induce

the CDW phase (Fig. 1). We have also shown that “pure” exciton condensation without lattice distortion is difficult (not realistic) in  $1T$ - $\text{TiSe}_2$ . This is in contrast to the case of two-dimensional square lattice, where the pure exciton condensation is widely observed using the same calculation method [2]. Our result suggests that the stability of exciton condensation greatly depends on the nesting condition of the Fermi surface in the normal state. We conclude that in  $1T$ - $\text{TiSe}_2$  with poor nesting condition, both electronic and lattice degrees of freedom are crucial for the understanding of the quantum phases.

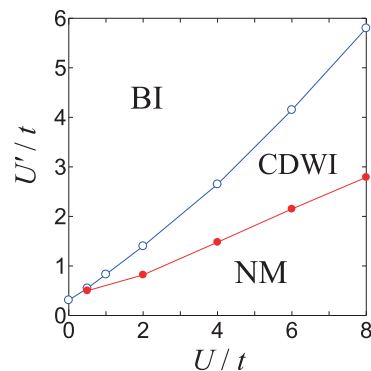


Figure 1: Ground state phase diagram for intraband ( $U$ ) and interband ( $U'$ ) Coulomb interactions with electron-lattice coupling  $g/t = 0.19$  [1]. NM, CDWI, and BI denote normal metal, charge-density wave insulator, and band insulator.

## References

- [1] H. Watanabe, K. Seki, and S. Yunoki:  
Phys. Rev. B **91** (2015) 205135.
- [2] H. Watanabe, K. Seki, and S. Yunoki: J.  
Phys.: Conf. Ser. **592** (2015) 012097.

# Chiral Magnetic Effect in Condensed Matter Systems

Hiroyuki FUJITA and Masaki OSHIKAWA

*Institute for Solid State Physics, University of Tokyo  
Kashiwa-no-ha, Kashiwa, Chiba 277-8581*

Interface between quantum field theory and condensed matter physics has been a source of many important developments. Weyl fermions and accompanying chiral anomaly is a particularly notable example. Chiral Magnetic Effect (CME), namely an induction of electric current parallel to the applied magnetic field, was predicted as one of the consequences of chiral anomaly. With the prediction and subsequent experimental confirmations of Weyl fermions realized in actual materials (“Weyl semimetals”), there has been a strong interest in observing the CME in these materials. However, there are several subtle issues to be addressed carefully, for the possible observation of the CME. One of them is that, it is shown rigorously that the electric current vanishes under a static magnetic field in the equilibrium. This still leaves the possibility that the CME can be observed at a non-vanishing frequency. Even if this is the case, another subtlety is that the electric and magnetic fields, and electric charge and current densities have to obey the laws of electrodynamics.

By solving the Maxwell-Chern-Simons (MCS) equations, we demonstrated that CME will qualitatively change transport properties of matter in rather unexpected ways [1]. We showed that the physically observed admittance is not simply proportional to the chiral magnetic conductivity  $\sigma_{\text{ch}}(\omega)$  as it has been expected, even when it is governed by the CME. Furthermore, we found that the CME-induced AC current is resonantly enhanced when the cross section matches the “chiral magnetic length”. Our results imply

that the electromagnetism is fundamental for actual transports in Weyl semimetals and that proposals for their applications to future electronics need careful considerations on this issue.

As a concrete setup, we considered the CME-capable Weyl semimetal in the solenoid as shown in Fig. 1. We focused on the CME-

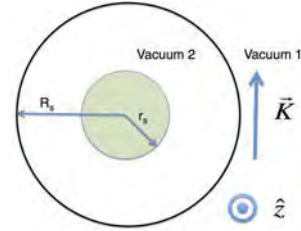


Figure 1: Schematic picture of our setup. A solenoid (radius  $R_s$ ) is represented as a surface current  $\mathbf{K}$  between the two vacua. Inside them, a cylindrical sample (radius  $r_s$ ) is placed.

dominant regime and discuss the leading order in the small- $\delta$  expansion, where

$$\delta = \frac{\omega\sigma}{\mu\sigma_{\text{ch}}^2}. \quad (1)$$

The admittance  $G$  of a cylinder with length  $L$  was determined as  $G = -i\omega C$ , where

$$C = \frac{iJ_z^{\text{tot}}}{\omega L E_z} \simeq \frac{2\pi}{\mu_0\omega^2 L \log\left[\frac{c}{\omega r_s}\right]}. \quad (2)$$

Namely, the admittance is universal and does not depend on material parameters.

Furthermore, the total current  $I_z^{\text{tot}}$  as a function of the external magnetic field  $\sim K$  was

obtained as

$$I_z^{\text{tot}} = \frac{\pi r_s J_0(\mu\sigma_{\text{ch}} r_s)}{\mu_0 J_1(\mu\sigma_{\text{ch}} r_s) \log\left[\frac{c}{\omega r_s}\right]} K + O\left(\frac{r_s}{R_s}\right). \quad (3)$$

This shows a resonant enhancement when  $J_1(\mu\sigma_{\text{ch}} r_s) \sim 0$ . In FIG. 2, we show  $I_z^{\text{tot}}$  for the following parameters:  $\mu\sigma_{\text{ch}} = 1 [\text{mm}^{-1}]$ ,  $\omega = 100 [\text{Hz}]$ ,  $B = 1 [\text{Gauss}]$  assuming  $r_s/R_s \simeq 0$ .

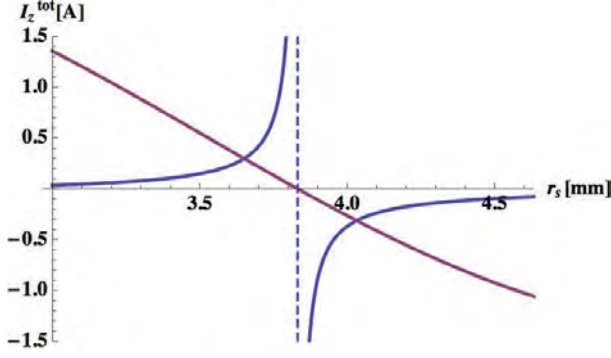


Figure 2: Blue line: Total current  $I_z^{\text{tot}} [\text{A}]$  for parameters  $\mu\sigma_{\text{ch}} = 1 [\text{mm}^{-1}]$ ,  $\omega = 100 [\text{Hz}]$ ,  $B = 1 [\text{Gauss}]$ . Red:  $J_1(\mu\sigma_{\text{ch}} r_s)$  in an arbitrary unit. The current is resonantly enhanced for  $r_s$  satisfying  $J_1(\mu\sigma_{\text{ch}} r_s) = 0$  represented by a dashed line.

While these results have been obtained analytically, we are now studying various aspects of the CME in more detail based on numerical calculations partially using the ISSP supercomputers.

## References

- [1] H. Fujita and M. Oshikawa, arXiv:1602.00687.